Electronic Research Archive

https://www.aimspress.com/journal/era

ERA, 34(8): 5452–5477.
DOI: 10.3934/era.2026244
Received: 22 May 2026
Revised: 22 June 2026
Accepted: 25 June 2026
Published: 30 June 2026

Research article

Order-reduced analysis and finite element approximation for a viscoelastic membrane equation with Caputo acceleration memory

Zhiwei Yang, Changyuan Chen, Wenrui Wang, Huaqing Ma and Yuan Ma*

School of Qilu Transportation, Shandong University, Jinan 250002, China

* **Correspondence:** Email: mayuan@sdu.edu.cn.

Abstract: We investigate the well-posedness, regularity, and numerical approximation of a viscoelastic membrane equation involving a Caputo fractional derivative of order $\alpha \in (1,2)$. The fractional term describes an acceleration history memory effect and is therefore different from the velocity memory damping terms commonly used in fractional viscoelastic wave models. By introducing the velocity variable $z = \partial_t u$ and setting $\beta = \alpha - 1$, the original problem is reformulated as an order-reduced first-order system in which a Caputo derivative of order $\beta \in (0,1)$ acts on the velocity. On the basis of this reformulation, we establish the well-posedness of the initial boundary value problem under homogeneous Neumann or Robin boundary conditions. For the Neumann case, a shifted spectral scale is introduced to include the zero eigenvalue and to obtain regularity estimates uniformly for both the constant and nonconstant modes. We then develop a fully discrete finite element method by combining continuous piecewise linear finite elements in space with the L1 approximation in time. Under suitable regularity and compatibility assumptions, we prove the error estimate

$$\|u - U\|_{\widehat{L^\infty}(L^2)} + \|\partial_t u - Z\|_{\widehat{L^\infty}(L^2)} \le C(\tau + h^2).$$

Numerical experiments are presented to confirm the predicted first-order temporal convergence and optimal second-order spatial convergence in the L^2 norm. In addition to the Neumann case, a Robin boundary manufactured solution test is included to demonstrate the applicability of the proposed framework under homogeneous Robin boundary conditions. Additional simulations illustrate the influence of the fractional order on viscoelastic membrane vibration and demonstrate the applicability of the proposed method to modal response analysis.

Keywords: Caputo fractional derivative; acceleration memory; viscoelastic membrane; fractional wave equation; finite element method; L1 scheme; modal analysis

1. Introduction

The mathematical modeling of vibrating membranes, beams, plates, and other elastic structures interacting with viscoelastic media is a classical topic in structural dynamics, continuum mechanics, and applied mathematics. Such models arise in vibration control, nondestructive testing, geophysical exploration, vehicle–track interactions, biomechanical systems, and composite materials; see, for example, [1–4]. Unlike ideal elastic media, viscoelastic materials exhibit hereditary effects, where the current response depends not only on the present state but also on the past deformation history. This feature has been extensively studied in classical continuum mechanics [5–7].

Fractional calculus provides a powerful and flexible tool for describing memory effects in complex media. Fractional constitutive laws can capture power-law relaxation, weakly singular kernels, and long-time temporal correlations with relatively few material parameters. The use of fractional derivatives in viscoelasticity dates back to the seminal works of Bagley and Torvik [8, 9], and has since been developed in many mechanical and rheological models; see [10–14]. For the general theory of fractional calculus and fractional differential equations, we refer to [15–19]. Compared with classical Kelvin–Voigt or Maxwell models, fractional models often better describe materials whose relaxation behavior is neither purely exponential nor adequately represented by finitely many integer-order internal variables.

In this paper, we study a viscoelastic membrane equation involving a Caputo fractional derivative of order $\alpha \in (1, 2)$. Let $\Omega \subset \mathbb{R}^d$, $d = 1, 2, 3$, be a bounded Lipschitz domain and let $T > 0$. The governing equation is

$$\eta(\boldsymbol{x})\partial_t^2 u + \mu(\boldsymbol{x})^C D_{0+}^{\alpha} u + \mathcal{A}u = F \quad \text{in } \Omega \times (0, T), \tag{1.1}$$

where η and μ are positive coefficients, F is a prescribed source term, and

$$\mathcal{A}\varphi = -\operatorname{div}(\boldsymbol{A}(\boldsymbol{x})\nabla\varphi) + c(\boldsymbol{x})\varphi.$$

Here, $\boldsymbol{A}$ is uniformly positive definite and $c(\boldsymbol{x}) \geq 0$. The conormal derivative is denoted by as $\partial_{\boldsymbol{A}}\varphi = \boldsymbol{A}\nabla\varphi \cdot \boldsymbol{\nu}$, where $\boldsymbol{\nu}$ is the unit outward normal vector on $\partial\Omega$. We impose the homogeneous Neumann or Robin boundary condition

$$\partial_{\boldsymbol{A}} u + \sigma u = 0 \quad \text{on } \partial\Omega \times (0, T).$$

For $\gamma > 0$, the Riemann–Liouville fractional integral is defined by

$$J_{0+}^{\gamma} f(t) = \int_0^t \frac{(t-s)^{\gamma-1}}{\Gamma(\gamma)} f(s)\,\mathrm{d}s.$$

For $1 < \alpha < 2$, the Caputo derivative used in this work is

$${}^C D_{0+}^{\alpha} u(t) = J_{0+}^{2-\alpha}\partial_t^2 u(t) = \int_0^t \frac{(t-s)^{1-\alpha}}{\Gamma(2-\alpha)}\partial_s^2 u(s)\,\mathrm{d}s.$$

Thus the fractional term in (1.1) represents a memory effect generated by the acceleration history. This differs from velocity memory models involving, for example, $J_{0+}^{2-\alpha}\partial_t u$ or fractional derivatives acting directly on the velocity. This distinction leads to different regularity structures, compatibility requirements near $t = 0$, and consistency terms in time discretization. From the viewpoint of structural dynamics, the acceleration history term can be interpreted as a fractional hereditary inertia or delayed dynamic response in viscoelastic media.

The mathematical analysis and numerical approximation of fractional evolution equations have attracted considerable attention. For time-fractional diffusion and subdiffusion equations, important progress has been made on finite difference methods, spectral methods, finite element methods, convolution quadrature, and L1-type schemes; see [20–27]. These studies reveal typical features of fractional evolution problems, including weak initial singularities, reduced temporal regularity, and the need for carefully designed consistency and stability estimates.

More recently, robust time-stepping methods on nonuniform meshes, discrete fractional Gronwall inequalities, and high-order convolution-type discretizations have been developed. Representative results include stability and convergence analyses for L2-type or L1-type methods on nonuniform meshes [28, 29], corrected and high-order convolution quadrature methods for fractional evolution equations [21, 30], and finite element or convolution quadrature approximations for nonlinear and quasilinear subdiffusion models [31]. Most of these works, however, focus on subdiffusion-type problems with fractional order in $(0, 1)$.

For fractional diffusion-wave and wave-type equations with a derivative order between one and two, the analysis is more delicate because hyperbolic propagation is coupled with nonlocal temporal memory. Related numerical studies include finite difference, spectral, discontinuous Galerkin, and finite element methods for diffusion wave, variable-order fractional, and fractional wave equations [32–34]. Recent computational work on fractional viscoelastic wave propagation also demonstrates the practical importance of efficient fully discrete schemes for fractional constitutive models [35]. Recent studies on variable-order and variable-exponent fractional models include variable-order fractional wave equations [36], hidden-memory variable-order fractional optimal control and diffusion models [37, 38], optimal-order approximations for variable-order time- and space-fractional diffusion equations [39, 40], variable-exponent fractional problems [41], and time-fractional mean field control models [42].

Despite these advances, the acceleration memory membrane equation (1.1) has not been fully addressed from the viewpoint of well-posedness, Neumann-compatible regularity, and finite element error analysis. The main difficulties are threefold. First, the Caputo derivative has the order $\alpha \in (1, 2)$ and acts on the displacement through its second time derivative. Second, under Neumann boundary conditions, the elliptic operator may have a zero eigenvalue, so standard spectral scales based only on positive eigenvalues do not directly handle the constant mode. Third, the numerical method must approximate the acceleration history memory term consistently rather than a velocity memory term.

The present model is not a direct specialization of standard time fractional diffusion wave equations. In many fractional damping models, the memory term is imposed on the velocity or on a strain-related variable. In contrast, the Caputo term in (1.1) is generated by the acceleration history. Introducing $z = \partial_t u$ and $\beta = \alpha - 1$, we have

$$ {}^{C}D^{\alpha}_{0+}u = J^{2-\alpha}_{0+}\partial^2_t u = J^{1-\beta}_{0+}\partial_t z = {}^{C}D^{\beta}_{0+}z. $$

Consequently, (1.1) can be rewritten as the order-reduced system

$$ \begin{cases} \eta\partial_t z + \mu {}^{C}D^{\beta}_{0+}z + \mathcal{A}u = F, & \text{in } \Omega \times (0, T), \\ \partial_t u = z, & \text{in } \Omega \times (0, T). \end{cases} $$

This formulation is the main analytical and numerical device of this paper. It allows us to exploit positivity properties of Caputo derivatives of order less than one and leads naturally to an L1 time discretization for the velocity variable.

The main contributions of this work are summarized as follows.

- We formulate a viscoelastic membrane model with a Caputo derivative of order $\alpha \in (1, 2)$, where the fractional term represents an acceleration history memory effect, and derive an order-reduced system by introducing the velocity variable with $\beta = \alpha - 1 \in (0, 1)$.
- We establish the well-posedness of the initial-boundary value problem under homogeneous Neumann or Robin boundary conditions, and develop a shifted spectral scale to handle the zero eigenvalue in the Neumann case.
- We construct a fully discrete finite element method using continuous piecewise linear elements in space and the L1 approximation in time, and prove an $O(\tau + h^2)$ error estimate in the maximum-in-time L^2 norm.
- We provide numerical experiments, including convergence tests, Robin boundary and nonzero initial velocity verifications, fractional order-dependent vibration simulations, and modal response analysis.

The rest of the paper is organized as follows. Section 2 presents the forward problem and establishes its well-posedness. Section 3 develops the spectral regularity theory adapted to Neumann boundary conditions. Section 4 introduces the fully discrete finite element method and proves the error estimate. Section 5 presents numerical experiments, including manufactured solution tests, tests with a nonzero initial velocity and Robin boundary conditions, dynamic simulations, and modal response analysis. Finally, Section 6 concludes the paper.

2. Forward problem and well-posedness

2.1. Functional setting

Let $H = L^2(\Omega)$ and $V = H^1(\Omega)$. The bilinear form associated with the elliptic operator and the boundary contribution is defined by

$$a(\varphi, \chi) = \int_\Omega \boldsymbol{A}\nabla\varphi \cdot \nabla\chi \, \mathrm{d}\boldsymbol{x} + \int_\Omega c\varphi\chi \, \mathrm{d}\boldsymbol{x} + \int_{\partial\Omega} \sigma\varphi\chi \, \mathrm{d}S.$$

We assume that there exist constants $c_0 > 0$ and $\gamma \geq 0$ such that

$$a(v, v) + \gamma\|v\|^2_{L^2(\Omega)} \geq c_0\|v\|^2_{H^1(\Omega)}, \qquad \forall v \in V. \tag{2.1}$$

In the case of a pure Neumann Laplacian, coercivity holds only modulo constants. This does not create difficulties on finite time intervals, because the constant mode is controlled by the initial displacement and velocity.

The weak formulation is to find

$$u \in L^\infty(0, T; V), \qquad \partial_t u \in L^\infty(0, T; H),$$

such that, for almost every $t \in (0, T)$, we have

$$\langle \eta\partial_t^2 u, \chi\rangle_{V',V} + (\mu\, {}^C D^\alpha_{0+} u, \chi) + a(u, \chi) = (F, \chi), \qquad \forall \chi \in V. \tag{2.2}$$

2.2. Order-reduced formulation

Let $z = \partial_t u$ and $\beta = \alpha - 1 \in (0,1)$. Since

$$^{C}D^{\alpha}_{0+}u = J^{2-\alpha}_{0+}\partial_t^2 u = J^{1-\beta}_{0+}\partial_t z = {}^{C}D^{\beta}_{0+}z,$$

the original problem is equivalent to

$$\begin{cases} \eta\partial_t z + \mu{}^{C}D^{\beta}_{0+}z + \mathcal{A}u = F, & \text{in } \Omega\times(0,T),\\ \partial_t u = z, & \text{in } \Omega\times(0,T),\\ u(\cdot,0) = u_0, \quad z(\cdot,0) = u_1. & \end{cases} \tag{2.3}$$

2.3. Positivity of the fractional term

The following positivity property follows from the positive definiteness of the fractional convolution kernel.

Lemma 2.1. *Let $0 < \beta < 1$. If $\phi \in H^1(0,T;H)$ and $\phi(0) = 0$, then*

$$\int_0^T ({}^{C}D^{\beta}_{0+}\phi(t), \phi(t))_H \,\mathrm{d}t \geq 0. \tag{2.4}$$

Proof. Since $\phi(0) = 0$, the Caputo derivative coincides with the Riemann–Liouville derivative in the weak sense. Extending ϕ by zero outside $(0,T)$ and applying the Fourier transform in time, one obtains

$$\int_0^T ({}^{C}D^{\beta}_{0+}\phi(t), \phi(t))_H \,\mathrm{d}t = c_\beta \int_{\mathbb{R}} |\xi|^\beta \|\widehat{\phi}(\xi)\|_H^2 \,\mathrm{d}\xi,$$

where $c_\beta > 0$. This proves the claim.

Remark 2.2. *If the initial velocity is nonzero, one may write $z = u_1 + \widetilde{z}$ with $\widetilde{z}(0) = 0$. Since the Caputo derivative of a time-independent function vanishes,*

$$^{C}D^{\beta}_{0+}z = {}^{C}D^{\beta}_{0+}\widetilde{z}.$$

Hence, the positivity estimate applies to the principal fractional contribution, while the remaining terms can be controlled by Young's inequality.

2.4. Well-posedness

Theorem 2.3. *Assume that $F \in L^2(0,T;H)$, $u_0 \in V$, and $u_1 \in H$. Suppose further that*

$$0 < \eta_0 \leq \eta(\boldsymbol{x}) \leq \eta_1, \qquad 0 < \mu_0 \leq \mu(\boldsymbol{x}) \leq \mu_1$$

almost everywhere in Ω. Then the initial-boundary value problem admits a unique weak solution satisfying

$$u \in L^\infty(0,T;V), \qquad \partial_t u \in L^\infty(0,T;H).$$

Moreover,

$$\|u\|_{L^\infty(0,T;V)} + \|\partial_t u\|_{L^\infty(0,T;H)} \leq C\left(\|F\|_{L^2(0,T;H)} + \|u_0\|_V + \|u_1\|_H\right), \tag{2.5}$$

where $C > 0$ is independent of F, u_0, and u_1.

Proof. Let $\{\phi_j\}_{j=1}^{\infty}$ be a basis of V that is orthonormal in H, and set $V_N = \text{span}\{\phi_1, \ldots, \phi_N\}$. We seek for the approximate solutions

$$u_N(t) = \sum_{j=1}^{N} d_j^N(t)\phi_j, \qquad z_N(t) = \partial_t u_N(t),$$

satisfying

$$(\eta\partial_t z_N, \chi_N) + (\mu {}^C D_{0+}^{\beta} z_N, \chi_N) + a(u_N, \chi_N) = (F, \chi_N), \qquad \forall \chi_N \in V_N. \tag{2.6}$$

Taking $\chi_N = z_N$ and using $\partial_t u_N = z_N$ yield

$$\frac{1}{2}\frac{\mathrm{d}}{\mathrm{d}t}\|\sqrt{\eta} z_N(t)\|_{L^2}^2 + (\mu {}^C D_{0+}^{\beta} z_N, z_N) + \frac{1}{2}\frac{\mathrm{d}}{\mathrm{d}t} a(u_N(t), u_N(t)) = (F, z_N). \tag{2.7}$$

Taking $z_N = z_N(0) + \widetilde{z}_N$ with $\widetilde{z}_N(0) = 0$, Lemma 2.1 implies the nonnegativity of the principal fractional contribution after integration in time. Young's inequality then gives

$$\|\sqrt{\eta} z_N(t)\|_{L^2}^2 + a(u_N(t), u_N(t)) \le C\left(\|u_{0,N}\|_V^2 + \|u_{1,N}\|_{L^2}^2 + \int_0^t \|F(s)\|_{L^2}^2 \,\mathrm{d}s\right) + C\int_0^t \|z_N(s)\|_{L^2}^2 \,\mathrm{d}s.$$

Combining this estimate with (2.1) and Gronwall's inequality yields uniform bounds for u_N in $L^\infty(0, T; V)$ and for z_N in $L^\infty(0, T; H)$.

In the pure Neumann case, the constant mode is controlled by

$$\|u_N(t)\|_{L^2} \le \|u_N(0)\|_{L^2} + \int_0^t \|z_N(s)\|_{L^2} \,\mathrm{d}s.$$

The Galerkin equation further provides a bound for $\partial_t z_N$ in a suitable dual space. Standard compactness arguments then allow passage to the limit and yield existence. Uniqueness follows by applying the same energy estimate to the difference of two solutions.

3. Spectral regularity under Neumann boundary conditions

In this section, we focus on the self-adjoint case $\eta \equiv 1$ and $\mu \equiv k > 0$. We assume that $\mathcal{A}$ is a nonnegative self-adjoint elliptic operator subject to homogeneous Neumann or Robin boundary conditions. The spectral framework below is standard for self-adjoint elliptic operators; see, for example, [43].

Let $\{(\Lambda_j, \phi_j)\}_{j=0}^{\infty}$ be the eigenpairs of $\mathcal{A}$, namely

$$\mathcal{A}\phi_j = \Lambda_j\phi_j, \qquad 0 = \Lambda_0 \le \Lambda_1 \le \Lambda_2 \le \cdots, \qquad \Lambda_j \to +\infty.$$

The eigenfunctions $\{\phi_j\}_{j=0}^{\infty}$ form an orthonormal basis of $L^2(\Omega)$. To treat the zero Neumann mode and the positive modes uniformly, we define

$$\rho_j = (1 + \Lambda_j)^{1/2}.$$

For $m \ge 0$, introduce

$$\check{H}_N^m(\Omega) = \left\{ v \in L^2(\Omega) : \|v\|_{\check{H}_N^m}^2 = \sum_{j=0}^{\infty} \rho_j^{2m}(v, \phi_j)^2 < \infty \right\}. \tag{3.1}$$

Expanding

$$u(\boldsymbol{x},t)=\sum_{j=0}^{\infty}u_j(t)\phi_j(\boldsymbol{x}), \qquad F(\boldsymbol{x},t)=\sum_{j=0}^{\infty}f_j(t)\phi_j(\boldsymbol{x}),$$

gives

$$u_j''(t)+k{}^CD_{0+}^{\alpha}u_j(t)+\Lambda_j u_j(t)=f_j(t), \qquad u_j(0)=u_{0,j}, \quad u_j'(0)=u_{1,j}. \tag{3.2}$$

Equivalently, with $z_j=u_j'$ and $\beta=\alpha-1$, we have

$$z_j'(t)+k{}^CD_{0+}^{\beta}z_j(t)+\Lambda_j u_j(t)=f_j(t), \qquad u_j'(t)=z_j(t). \tag{3.3}$$

Lemma 3.1. *Let* $1<\alpha<2$, $k>0$, *and* $f_j\in H^1(0,T)$. *Then* (3.2) *admits a unique solution satisfying*

$$\|u_j\|_{C^m[0,T]}\le C\left(\rho_j^m|u_{0,j}|+\rho_j^{m-1}|u_{1,j}|+\rho_j^{m-2}\|f_j\|_{H^1(0,T)}\right), \qquad m=1,2. \tag{3.4}$$

If $f_j\in C^1[0,T]$, *then* $u_j'''\in C(0,T]$ *and*

$$|u_j'''(t)|\le C\left(\rho_j^3|u_{0,j}|+\rho_j^2|u_{1,j}|+\rho_j\|f_j\|_{H^1(0,T)}+|f_j'(t)|+t^{1-\alpha}|u_{1,j}|\right) \tag{3.5}$$

for $0<t\le T$.

Proof. For positive modes, taking the Laplace transform of (3.2) gives the transformed equation explicitly. Since $1<\alpha<2$, the Laplace transform of the Caputo derivative is

$$\mathcal{L}\left\{{}^CD_{0+}^{\alpha}u_j(t)\right\}(s)=s^{\alpha}\widehat{u_j}(s)-s^{\alpha-1}u_{0,j}-s^{\alpha-2}u_{1,j}.$$

Moreover,

$$\mathcal{L}\{u_j''(t)\}(s)=s^2\widehat{u_j}(s)-su_{0,j}-u_{1,j}.$$

Therefore, applying the Laplace transform to

$$u_j''(t)+k{}^CD_{0+}^{\alpha}u_j(t)+\Lambda_j u_j(t)=f_j(t)$$

yields

$$\left(s^2+ks^{\alpha}+\Lambda_j\right)\widehat{u_j}(s)=su_{0,j}+u_{1,j}+ks^{\alpha-1}u_{0,j}+ks^{\alpha-2}u_{1,j}+\widehat{f_j}(s).$$

Consequently,

$$\widehat{u_j}(s)=\frac{su_{0,j}+u_{1,j}+ks^{\alpha-1}u_{0,j}+ks^{\alpha-2}u_{1,j}+\widehat{f_j}(s)}{s^2+ks^{\alpha}+\Lambda_j}.$$

The denominator satisfies standard sectorial lower bounds on suitable contours in the complex plane. Inverting the Laplace transform and using the corresponding resolvent estimates for scalar fractional wave equations yield the stated frequency-dependent bounds. These arguments are standard in the theory of fractional evolution equations. The use of the shifted frequency $\rho_j=(1+\Lambda_j)^{1/2}$ allows the estimates to be written uniformly with respect to all modes.

For the zero Neumann mode, the equation reduces to

$$z_0'(t)+k{}^CD_{0+}^{\beta}z_0(t)=f_0(t), \qquad z_0(0)=u_{1,0}.$$

This is a scalar Volterra equation with a weakly singular kernel. Standard Volterra estimates give the same bounds with $\rho_0=1$. The term $t^{1-\alpha}$ represents the weak initial singularity generated by the fractional derivative.

Theorem 3.2. *Assume that*

$$u_0 \in \check{H}_N^2(\Omega), \qquad u_1 \in \check{H}_N^1(\Omega), \qquad F \in H^1(0,T;L^2(\Omega)).$$

Then

$$u \in C^2([0,T];L^2(\Omega)) \cap C([0,T];\check{H}_N^2(\Omega)),$$

and

$$\|u\|_{C^2([0,T];L^2)} + \|u\|_{C([0,T];\check{H}_N^2)} \le C\left(\|u_0\|_{\check{H}_N^2} + \|u_1\|_{\check{H}_N^1} + \|F\|_{H^1(0,T;L^2)}\right). \tag{3.6}$$

If, in addition, we have

$$u_0 \in \check{H}_N^3(\Omega), \qquad u_1 \in \check{H}_N^2(\Omega), \qquad F \in H^1(0,T;\check{H}_N^1(\Omega)) \cap C^1([0,T];L^2(\Omega)),$$

then $u \in C^3((0,T];L^2(\Omega))$ and

$$\|\partial_t^3 u(\cdot,t)\|_{L^2(\Omega)} \le C\left(\mathcal{M} + t^{1-\alpha}\|u_1\|_{L^2(\Omega)}\right), \qquad 0 < t \le T, \tag{3.7}$$

where

$$\mathcal{M} = \|u_0\|_{\check{H}_N^3} + \|u_1\|_{\check{H}_N^2} + \|F\|_{H^1(0,T;\check{H}_N^1)} + \|F\|_{C^1([0,T];L^2)}.$$

Consequently, we have

$$\int_0^T \|\partial_t^3 u(\cdot,t)\|_{L^2(\Omega)}\,\mathrm{d}t \le C\left(\mathcal{M}T + \frac{T^{2-\alpha}}{2-\alpha}\|u_1\|_{L^2(\Omega)}\right). \tag{3.8}$$

Proof. The assertion follows by applying Lemma 3.1 to each Fourier coefficient and summing over all modes. For example,

$$\sum_{j=0}^{\infty} \|u_j''\|_{C[0,T]}^2 \le C \sum_{j=0}^{\infty}\left(\rho_j^4|u_{0,j}|^2 + \rho_j^2|u_{1,j}|^2 + \|f_j\|_{H^1(0,T)}^2\right),$$

which yields the $C^2([0,T];L^2)$ estimate. The estimate in $C([0,T];\check{H}_N^2)$ is obtained similarly. The bound for $\partial_t^3 u$ follows from (3.5). Finally, we have

$$\int_0^T t^{1-\alpha}\,\mathrm{d}t = \frac{T^{2-\alpha}}{2-\alpha} < \infty,$$

which proves (3.8).

Remark 3.3. *The shifted spectral scale $\rho_j = (1+\Lambda_j)^{1/2}$ is essential for pure Neumann boundary conditions. It avoids singular behavior at the zero eigenvalue and enables the constant mode and the oscillatory modes to be handled within a single regularity framework.*

4. Finite element approximation and error analysis

4.1. Reduced formulation

In the self-adjoint setting of $\eta \equiv 1$ and $\mu \equiv k > 0$, the reduced problem reads

$$\begin{cases} \partial_t z + k\,{}^C D_{0+}^{\beta} z + \mathcal{A}u = F, & \text{in } \Omega \times (0,T), \\ \partial_t u = z, & \text{in } \Omega \times (0,T), \\ u(\cdot,0) = u_0, \quad z(\cdot,0) = u_1. \end{cases} \tag{4.1}$$

4.2. L1 approximation

Let $0 = t_0 < t_1 < \cdots < t_N = T$ be a uniform temporal partition with a time step $\tau = T/N$. For a sequence $\{W^n\}_{n=0}^{N}$, define

$$\delta_\tau W^n = \frac{W^n - W^{n-1}}{\tau}.$$

The L1 approximation of the Caputo derivative is defined by

$$(\mathcal{D}_\tau^\beta Z)^n = \frac{1}{\Gamma(2-\beta)\tau^\beta} \sum_{m=1}^{n} a_{n-m} \left(Z^m - Z^{m-1} \right), \tag{4.2}$$

where

$$a_\ell = (\ell + 1)^{1-\beta} - \ell^{1-\beta}, \qquad \ell = 0, 1, 2, \ldots. \tag{4.3}$$

Lemma 4.1. *Let* $0 < \beta < 1$. *If* $W^0 = 0$, *then*

$$\tau \sum_{n=1}^{N} \left((\mathcal{D}_\tau^\beta W)^n, W^n \right) \geq 0. \tag{4.4}$$

Proof. The L1 operator is generated by a positive definite convolution sequence. Equivalently, the symmetric part of the associated lower triangular Toeplitz matrix is positive semidefinite. This gives the discrete counterpart of Lemma 2.1; see, for example, [20, 23, 28].

Remark 4.2. *The L1 approximation used in this work is first-order accurate in time, but it has several advantages in the present order-reduced framework. First, it is simple to implement and leads to a positive definite convolution structure, which is useful for the stability analysis. Second, after the order reduction* $z = \partial_t u$ *and* $\beta = \alpha - 1 \in (0, 1)$, *the memory term becomes a subdiffusive Caputo derivative acting on the velocity variable, for which the L1 formula provides a robust baseline discretization. Third, the method is relatively robust for solutions with weak initial singularities, which commonly occur in fractional evolution equations.*

The order-reduced framework itself is not restricted to the L1 formula. In principle, higher-order convolution quadrature methods, Alikhanov-type schemes, or corrected high-order finite difference formulas can be applied to the reduced Caputo derivative of order β. *However, for fractional evolution equations, even smooth input data may generate weak singular behavior near* $t = 0$. *On uniform temporal meshes, such weak initial singularities may reduce the actually observed temporal convergence order of high-order schemes unless correction terms, graded meshes, or additional compatibility conditions are imposed. Therefore, the L1 method adopted here should be viewed as a stable and robust first-order baseline, while high-order extensions require a separate treatment of initial singularities and are left for future work.*

4.3. Fully discrete finite element scheme

Let $\mathcal{T}_h$ be a quasi-uniform triangulation of Ω, and let $S_h \subset H^1(\Omega)$ be the space of continuous piecewise linear finite elements. Since the Neumann problem may have a constant kernel, we use the shifted Ritz projection $\Pi_h : H^1(\Omega) \to S_h$ defined by

$$a(\Pi_h v, \chi_h) + (\Pi_h v, \chi_h) = a(v, \chi_h) + (v, \chi_h), \qquad \forall \chi_h \in S_h. \tag{4.5}$$

Under standard elliptic regularity, this projection satisfies

$$\|v - \Pi_h v\|_{L^2(\Omega)} + h\|v - \Pi_h v\|_{H^1(\Omega)} \leq Ch^2 \|v\|_{H^2(\Omega)}. \tag{4.6}$$

The fully discrete scheme is to find $U^n, Z^n \in S_h$ such that, for $1 \leq n \leq N$,

$$(\delta_\tau Z^n, \chi_h) + k((\mathcal{D}_\tau^\beta Z)^n, \chi_h) + a(U^n, \chi_h) = (F^n, \chi_h), \qquad \forall \chi_h \in S_h, \tag{4.7}$$

and

$$\delta_\tau U^n = Z^n. \tag{4.8}$$

The initial values are chosen as

$$U^0 = \Pi_h u_0, \qquad Z^0 = \Pi_h u_1. \tag{4.9}$$

4.4. Implementation

Let $\{\varphi_i\}_{i=1}^{M_h}$ be a basis of S_h. Define the mass and stiffness matrices by

$$\mathbf{M}_{ij} = (\varphi_j, \varphi_i), \qquad \mathbf{K}_{ij} = a(\varphi_j, \varphi_i).$$

Substituting $U^n = U^{n-1} + \tau Z^n$ into (4.7) yields

$$\begin{aligned}\left(\frac{1}{\tau}\mathbf{M} + \frac{k}{\Gamma(2-\beta)\tau^\beta}\mathbf{M} + \tau\mathbf{K}\right)\mathbf{Z}^n = \mathbf{F}^n + \left(\frac{1}{\tau}\mathbf{M} + \frac{k}{\Gamma(2-\beta)\tau^\beta}\mathbf{M}\right)\mathbf{Z}^{n-1} \\ - \frac{k}{\Gamma(2-\beta)\tau^\beta}\mathbf{M}\mathbf{H}^n - \mathbf{K}\mathbf{U}^{n-1},\end{aligned} \tag{4.10}$$

where

$$\mathbf{H}^n = \sum_{m=1}^{n-1} a_{n-m}\left(\mathbf{Z}^m - \mathbf{Z}^{m-1}\right), \qquad \mathbf{H}^1 = \mathbf{0}.$$

Once $\mathbf{Z}^n$ is obtained, the displacement is updated by

$$\mathbf{U}^n = \mathbf{U}^{n-1} + \tau\mathbf{Z}^n.$$

Theorem 4.3. *For any $h > 0$ and $\tau > 0$, the fully discrete scheme* (4.7)–(4.8) *admits a unique solution.*

Proof. At each time level, the scheme is equivalent to the linear system (4.10). The coefficient matrix consists of a positive definite mass contribution, the positive L1 diagonal contribution, and the non-negative stiffness contribution. Therefore, it is nonsingular. Once Z^n has been determined, U^n is uniquely obtained from (4.8).

Algorithm 1 Fully discrete L1 finite element method

Require: Mesh $\mathcal{T}_h$, final time T, time step τ, fractional order $\alpha \in (1,2)$, initial data u_0, u_1, and source term F.

Ensure: Numerical solutions $\{U^n, Z^n\}_{n=0}^N$.

Set $\beta = \alpha - 1$ and $N = T/\tau$.

Construct the finite element space S_h.

Assemble the mass matrix $\mathbf{M}$ and stiffness matrix $\mathbf{K}$.

Compute the initial vectors $\mathbf{U}^0$ and $\mathbf{Z}^0$ from $U^0 = \Pi_h u_0$ and $Z^0 = \Pi_h u_1$.

Precompute the L1 weights $a_\ell = (\ell+1)^{1-\beta} - \ell^{1-\beta}$ for $\ell = 0, \ldots, N-1$.

Set $\kappa = k/(\Gamma(2-\beta)\tau^\beta)$.

for $n = 1, 2, \ldots, N$ **do**

Compute the history vector

$$\mathbf{H}^n = \sum_{m=1}^{n-1} a_{n-m}\left(\mathbf{Z}^m - \mathbf{Z}^{m-1}\right).$$

Assemble the right-hand side

$$\mathbf{b}^n = \mathbf{F}^n + \left(\frac{1}{\tau}\mathbf{M} + \kappa\mathbf{M}\right)\mathbf{Z}^{n-1} - \kappa\mathbf{M}\mathbf{H}^n - \mathbf{K}\mathbf{U}^{n-1}.$$

Solve

$$\left(\frac{1}{\tau}\mathbf{M} + \kappa\mathbf{M} + \tau\mathbf{K}\right)\mathbf{Z}^n = \mathbf{b}^n.$$

Update

$$\mathbf{U}^n = \mathbf{U}^{n-1} + \tau\mathbf{Z}^n.$$

end for

4.5. Consistency estimates

For a sequence $\{W^n\}_{n=0}^N$, define

$$\|W\|_{\widehat{L^\infty}(L^2)} = \max_{0\le n\le N} \|W^n\|_{L^2(\Omega)}. \tag{4.11}$$

Let $z = \partial_t u$. Define

$$\widehat{E^n} = \delta_\tau u(t_n) - z(t_n), \tag{4.12}$$

$$E^n = \delta_\tau z(t_n) - \partial_t z(t_n), \tag{4.13}$$

and

$$R^n = {}^C D_{0+}^\beta z(t_n) - (\mathcal{D}_\tau^\beta z)^n. \tag{4.14}$$

Lemma 4.4. *Assume that*

$$u_0 \in \check{H}_N^4(\Omega), \qquad u_1 \in \check{H}_N^3(\Omega),$$

and

$$F \in H^1(0,T; \check{H}_N^2(\Omega)) \cap C^1([0,T]; L^2(\Omega)).$$

Assume further also that the compatibility conditions are sufficient to guarantee the L1 consistency estimate

$$\tau \sum_{n=1}^{N} \|R^n\|_{L^2(\Omega)} \le C\mathcal{M}\tau, \tag{4.15}$$

where

$$\mathcal{M} = \|u_0\|_{\check{H}_N^4} + \|u_1\|_{\check{H}_N^3} + \|F\|_{H^1(0,T;\check{H}_N^2)} + \|F\|_{C^1([0,T];L^2)}.$$

Then

$$\|\widehat{E}\|_{\widehat{L^\infty}(L^2)} \le C\mathcal{M}\tau, \tag{4.16}$$

and

$$\tau \sum_{n=1}^{N} \|E^n\|_{L^2(\Omega)} \le C\mathcal{M}\tau. \tag{4.17}$$

Proof. Taylor's formula gives

$$\widehat{E}^n = -\frac{1}{\tau} \int_{t_{n-1}}^{t_n} (t - t_{n-1}) \partial_t z(t)\, \mathrm{d}t.$$

The regularity result in Theorem 3.2 implies (4.16). Similarly,

$$E^n = -\frac{1}{\tau} \int_{t_{n-1}}^{t_n} (t - t_{n-1}) \partial_t^3 u(t)\, \mathrm{d}t,$$

and hence

$$\tau \sum_{n=1}^{N} \|E^n\|_{L^2} \le C\tau \int_0^T \|\partial_t^3 u(t)\|_{L^2}\, \mathrm{d}t \le C\mathcal{M}\tau.$$

The estimate (4.15) follows from the local truncation error representation of the L1 approximation. More precisely, on each interval (t_{m-1}, t_m), the error is expressed in terms of the difference between $z'(s)$ and its cell average. The regularity estimate for $\partial_t^3 u$ in Theorem 3.2, together with the integrability of the weak singular factor $t^{1-\alpha}$, yields the accumulated bound (4.15); see also [20, 22, 24, 27].

4.6. Error estimate

Theorem 4.5. *Let* (u, z) *be the solution of* (4.1)*, and let* $\{U^n, Z^n\}_{n=0}^N$ *be the numerical solution of* (4.7)–(4.8)*. Under the assumptions of Lemma 4.4, there is a constant* $C > 0$*, independent of* h *and* τ*, such that*

$$\|u - U\|_{\widehat{L^\infty}(L^2)} + \|z - Z\|_{\widehat{L^\infty}(L^2)} \le C\mathcal{M}(\tau + h^2). \tag{4.18}$$

Equivalently,

$$\|u - U\|_{\widehat{L^\infty}(L^2)} + \|\partial_t u - Z\|_{\widehat{L^\infty}(L^2)} \le C\mathcal{M}(\tau + h^2). \tag{4.19}$$

Proof. Decompose the displacement error as

$$u(t_n) - U^n = \widehat{\eta}^n + \widehat{\xi}^n, \qquad \widehat{\eta}^n = u(t_n) - \Pi_h u(t_n), \qquad \widehat{\xi}^n = \Pi_h u(t_n) - U^n,$$

and the velocity error as

$$z(t_n) - Z^n = \eta^n + \xi^n, \qquad \eta^n = z(t_n) - \Pi_h z(t_n), \qquad \xi^n = \Pi_h z(t_n) - Z^n.$$

The projection estimate (4.6) yields

$$\|\widehat{\eta}^n\|_{L^2} + \|\eta^n\|_{L^2} \le C\mathcal{M}h^2. \tag{4.20}$$

Subtracting the fully discrete scheme from the projected continuous equations gives

$$(\delta_\tau \xi^n, \chi_h) + k((\mathcal{D}_\tau^\beta \xi)^n, \chi_h) + a(\widehat{\xi}^n, \chi_h) = \mathcal{R}^n(\chi_h), \tag{4.21}$$

where $\mathcal{R}^n$ consists of the projection error, the L1 consistency error, and the backward Euler truncation error. Moreover,

$$\delta_\tau \widehat{\xi}^n = \xi^n + \eta^n - \delta_\tau \widehat{\eta}^n - \widehat{E}^n. \tag{4.22}$$

Taking $\chi_h = \xi^n$ in (4.21) and using (4.22), we obtain

$$\begin{aligned} &\|\xi^n\|_{L^2}^2 + \|\widehat{\xi}^n\|_a^2 - \|\xi^{n-1}\|_{L^2}^2 - \|\widehat{\xi}^{n-1}\|_a^2 + 2k\tau((\mathcal{D}_\tau^\beta \xi)^n, \xi^n) \\ &\le C\tau\left(\|\xi^n\|_{L^2}^2 + \|\widehat{\xi}^n\|_a^2\right) + C\tau\mathcal{M}^2(\tau^2 + h^4) + C\tau\left(\|E^n\|_{L^2} + \|R^n\|_{L^2}\right)\|\xi^n\|_{L^2}. \end{aligned} \tag{4.23}$$

Here, $\|\cdot\|_a$ denotes the seminorm induced by $a(\cdot,\cdot)$. Since the initial errors vanish, Lemma 4.1 implies that the accumulated fractional term is non-negative. Summing (4.23) over time levels and applying Lemma 4.4 yield

$$\|\xi^n\|_{L^2}^2 + \|\widehat{\xi}^n\|_a^2 \le C\mathcal{M}^2(\tau^2 + h^4) + C\tau \sum_{m=1}^{n} \left(\|\xi^m\|_{L^2}^2 + \|\widehat{\xi}^m\|_a^2\right).$$

The discrete Gronwall inequality then gives

$$\|\xi^n\|_{L^2} + \|\widehat{\xi}^n\|_a \le C\mathcal{M}(\tau + h^2).$$

Combining this estimate with (4.20) proves (4.18). Since $z = \partial_t u$, (4.19) follows.

5. Numerical experiments

This section presents five numerical experiments. Examples 1–3 are manufactured-solution tests for homogeneous Neumann boundary conditions, homogeneous Robin boundary conditions, and nonzero initial velocity, respectively. Example 4 studies the influence of the fractional order on membrane vibration, and Example 5 illustrates the modal response of the fractional viscoelastic membrane.

Unless otherwise stated, we take

$$\Omega = (0,1)^2, \qquad \eta = \mu = 1, \qquad \mathcal{A} = -\Delta, \qquad \sigma = 0.$$

Thus homogeneous Neumann boundary conditions are imposed unless otherwise specified.

5.1. *Example 1: A manufactured solution with Neumann boundary conditions*

We first verify the convergence rates of the proposed fully discrete L1 finite element method. The computation is carried out on $\Omega = (0,1)^2$ with $T = 1$, $\eta = \mu = 1$, $\mathcal{A} = -\Delta$, and homogeneous Neumann boundary conditions. Unless otherwise stated, we take $\alpha = 1.5$.

The exact solution is prescribed as

$$u(x,y,t) = t^{4-\alpha}\cos(\pi x)\cos(\pi y),$$

with the velocity

$$\partial_t u(x,y,t) = (4-\alpha)t^{3-\alpha}\cos(\pi x)\cos(\pi y).$$

The spatial factor $\cos(\pi x)\cos(\pi y)$ has a zero normal derivative on $\partial\Omega$, and hence the homogeneous Neumann boundary condition is satisfied.

Substituting the exact solution into the governing equation gives

$$F(x,y,t) = \left[(4-\alpha)(3-\alpha)t^{2-\alpha} + \frac{\Gamma(5-\alpha)}{\Gamma(5-2\alpha)}t^{4-2\alpha} + 2\pi^2 t^{4-\alpha}\right]\cos(\pi x)\cos(\pi y),$$

where

$$ {}^C D_{0+}^{\alpha} t^{4-\alpha} = \frac{\Gamma(5-\alpha)}{\Gamma(5-2\alpha)}t^{4-2\alpha}, \qquad -\Delta(\cos(\pi x)\cos(\pi y)) = 2\pi^2\cos(\pi x)\cos(\pi y).$$

The errors are measured in the maximum-in-time L^2 norm as follows:

$$e_u = \max_{0\le n\le N}\|u(t_n) - U^n\|_{L^2(\Omega)}, \qquad e_z = \max_{0\le n\le N}\|\partial_t u(t_n) - Z^n\|_{L^2(\Omega)},$$

and we report the combined error $e = e_u + e_z$. For the temporal test, we fix $h = 1/100$ and refine the time step. For the spatial test, we take $N = 4000$ and refine the mesh.

Table 1. Temporal convergence results for Example 1 with $\alpha = 1.5$ and $h = 1/100$.

N	τ	e_u	e_z	$e = e_u + e_z$	Order
16	$6.2500e-02$	$1.3433e-02$	$7.7523e-02$	$9.0956e-02$	–
32	$3.1250e-02$	$7.1735e-03$	$4.1315e-02$	$4.8488e-02$	0.9075
64	$1.5625e-02$	$3.7119e-03$	$2.1501e-02$	$2.5213e-02$	0.9435
128	$7.8125e-03$	$1.8853e-03$	$1.1076e-02$	$1.2961e-02$	0.9599

Table 2. Spatial convergence results for Example 1 with $\alpha = 1.5$ and $N = 4000$.

N_x	h	e_u	e_z	$e = e_u + e_z$	Order
4	$2.5000e-01$	$4.4203e-02$	$1.5805e-01$	$2.0226e-01$	–
8	$1.2500e-01$	$1.2553e-02$	$4.5145e-02$	$5.7698e-02$	1.8096
12	$8.3333e-02$	$5.7237e-03$	$2.0811e-02$	$2.6534e-02$	1.9158
16	$6.2500e-02$	$3.2418e-03$	$1.1964e-02$	$1.5206e-02$	1.9352

Tables 1 and 2 show first-order convergence in time and second-order convergence in space, consistent with

$$\|u - U\|_{\widehat{L^\infty}(L^2)} + \|\partial_t u - Z\|_{\widehat{L^\infty}(L^2)} \le C(\tau + h^2).$$

Figure 1 displays the exact solution, numerical solution, and pointwise error at the final time.

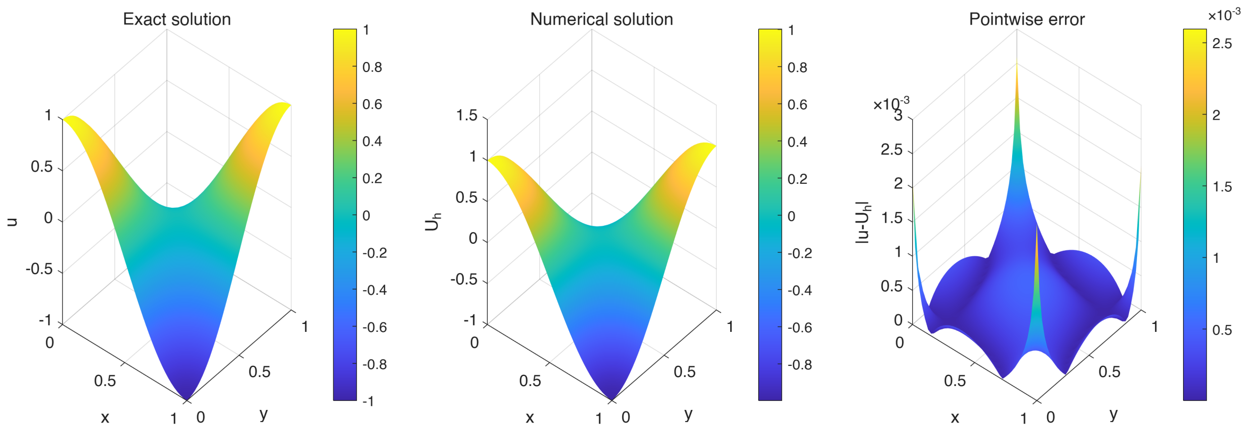

Figure 1. Exact solution, numerical solution, and pointwise error at the final time for Example 1.

5.2. Example 2: A manufactured solution with Robin boundary conditions

We next test the method under homogeneous Robin boundary conditions. The computation is carried out on $\Omega = (0,1)^2$ with $T = 1$, $\eta = \mu = 1$, and $\mathcal{A} = -\Delta$. We impose

$$\partial_\nu u + \sigma u = 0 \qquad \text{on } \partial\Omega \times (0,T).$$

Let

$$\lambda = \frac{\pi}{2}, \qquad \sigma = \lambda \tan\frac{\lambda}{2} = \frac{\pi}{2}, \qquad X(x) = \cos\left(\lambda\left(x - \frac{1}{2}\right)\right).$$

The exact solution is

$$u(x,y,t) = t^{4-\alpha} X(x) X(y).$$

Since

$$X'(0) = \lambda \sin\frac{\lambda}{2}, \qquad X'(1) = -\lambda \sin\frac{\lambda}{2}, \qquad X(0) = X(1) = \cos\frac{\lambda}{2},$$

the choice $\sigma = \lambda \tan(\lambda/2)$ gives $\partial_\nu u + \sigma u = 0$ on each side of the square.

The velocity is

$$\partial_t u(x,y,t) = (4-\alpha) t^{3-\alpha} X(x) X(y),$$

and the source term is

$$F(x,y,t) = \left[(4-\alpha)(3-\alpha)t^{2-\alpha} + \frac{\Gamma(5-\alpha)}{\Gamma(5-2\alpha)} t^{4-2\alpha} + 2\lambda^2 t^{4-\alpha}\right] X(x)X(y),$$

where

$$-\Delta\left(X(x)X(y)\right) = 2\lambda^2 X(x)X(y).$$

The errors are measured as in Example 1. For the temporal test, we fix $h = 1/100$ and refine the time step; for the spatial test, we use a sufficiently small time step and refine the mesh.

Tables 3 and 4 show the expected convergence behavior. A slight reductionin the observed spatial order on finer meshes may be due to the remaining temporal error. Overall, the results confirm that the order-reduced L1 finite element method also works effectively for homogeneous Robin boundary conditions.

Table 3. Temporal convergence results for the Robin boundary test with $\alpha = 1.5$ and $h = 1/100$.

N	τ	e_u	e_z	$e = e_u + e_z$	Order
16	6.2500e-02	6.3601e-02	5.1742e-02	1.1534e-01	–
32	3.1250e-02	3.2689e-02	2.6110e-02	5.8799e-02	0.9721
64	1.5625e-02	1.6571e-02	1.3163e-02	2.9734e-02	0.9837
128	7.8125e-03	8.3412e-03	6.6313e-03	1.4972e-02	0.9898

Table 4. Spatial convergence results for the Robin-boundary test with $\alpha = 1.5$ and $N = 8000$.

N_x	h	e_u	e_z	$e = e_u + e_z$	Order
4	2.5000e-01	4.7848e-03	1.5454e-02	2.0239e-02	–
8	1.2500e-01	1.2540e-03	4.2625e-03	5.5165e-03	1.8753
12	8.3333e-02	5.5089e-04	1.9759e-03	2.5268e-03	1.9257
16	6.2500e-02	3.0703e-04	1.1512e-03	1.4582e-03	1.9109

5.3. Example 3: A manufactured solution with nonzero initial velocity

We now consider a manufactured solution with a nonzero initial velocity. This test examines the accuracy of the scheme when the initial velocity contributes to the Caputo acceleration memory term. The computation is performed on $\Omega = (0,1)^2$ with $T = 1$, $\eta = \mu = 1$, $\mathcal{A} = -\Delta$, and homogeneous Neumann boundary conditions.

The exact solution is chosen as

$$u(x, y, t) = \left(t + t^{4-\alpha}\right) \cos(\pi x) \cos(\pi y).$$

Then

$$u(x, y, 0) = 0, \qquad \partial_t u(x, y, 0) = \cos(\pi x) \cos(\pi y),$$

so the initial velocity is nonzero. The velocity is

$$\partial_t u(x, y, t) = \left[1 + (4-\alpha)t^{3-\alpha}\right] \cos(\pi x) \cos(\pi y).$$

The homogeneous Neumann condition again follows from the spatial factor.

Substitution into

$$\partial_t^2 u + {}^C D_{0+}^{\alpha} u - \Delta u = F$$

gives

$$F(x, y, t) = \left[(4-\alpha)(3-\alpha)t^{2-\alpha} + \frac{\Gamma(5-\alpha)}{\Gamma(5-2\alpha)} t^{4-2\alpha} + 2\pi^2 \left(t + t^{4-\alpha}\right)\right] \cos(\pi x) \cos(\pi y),$$

where ${}^C D_{0+}^{\alpha} t = 0$ for $1 < \alpha < 2$.

The temporal and spatial convergence results are reported in Tables 5 and 6.

The results show that the proposed method remains stable and accurate for nonzero initial velocity, and the observed convergence behavior is consistent with the theoretical estimate.

Table 5. Temporal convergence results for Example 3 with a nonzero initial velocity, $\alpha = 1.5$, and $h = 1/100$.

N	τ	e_u	e_z	$e = e_u + e_z$	Order
16	6.2500e-02	1.3378e-02	7.7700e-02	9.1078e-02	–
32	3.1250e-02	7.1203e-03	4.1499e-02	4.8620e-02	0.9056
64	1.5625e-02	3.6613e-03	2.1691e-02	2.5352e-02	0.9394
128	7.8125e-03	1.8363e-03	1.1270e-02	1.3107e-02	0.9518

Table 6. Spatial convergence results for Example 3 with a nonzero initial velocity, $\alpha = 1.5$, and $N = 4000$.

N_x	h	e_u	e_z	$e = e_u + e_z$	Order
4	2.5000e-01	1.2243e-01	3.0298e-01	4.2540e-01	–
8	1.2500e-01	3.4746e-02	8.5578e-02	1.2032e-01	1.8219
12	8.3333e-02	1.5868e-02	3.9180e-02	5.5048e-02	1.9286
16	6.2500e-02	9.0089e-03	2.2370e-02	3.1379e-02	1.9538

5.4. Example 4: Effect of the fractional order on viscoelastic membrane vibration

This example illustrates the influence of the fractional order on the dynamic response of a viscoelastic membrane. We consider the homogeneous problem

$$\partial_t^2 u + k\,{}^C D_{0+}^{\alpha} u - \Delta u = 0 \quad \text{in } \Omega \times (0, T),$$

where

$$\Omega = (0,1)^2, \qquad T = 6, \qquad k = 0.6.$$

Homogeneous Neumann boundary conditions are imposed. The initial displacement is a localized perturbation

$$u_0(x,y) = \exp\left(-90\left((x-0.35)^2 + (y-0.5)^2\right)\right) - \overline{u}_0,$$

where $\overline{u}_0$ is the mass-weighted spatial average of the Gaussian profile. This removes the constant Neumann mode. The initial velocity is

$$\partial_t u(x,y,0) = 0,$$

and no external force is applied.

We test

$$\alpha = 1.2, \qquad \alpha = 1.5, \qquad \alpha = 1.8,$$

corresponding to

$$\beta = \alpha - 1 = 0.2, \qquad 0.5, \qquad 0.8.$$

The computation uses the proposed order-reduced L1 finite element method with continuous piecewise linear elements on a uniform triangular mesh.

Figure 2 shows the displacement at $(0.5, 0.5)$, Figure 3 shows the time evolution of the L^2 norm, and Figure 4 shows the final-time displacement profiles. The results indicate that the fractional order affects both the decay rate and the phase of the oscillatory response, as well as the final spatial distribution.

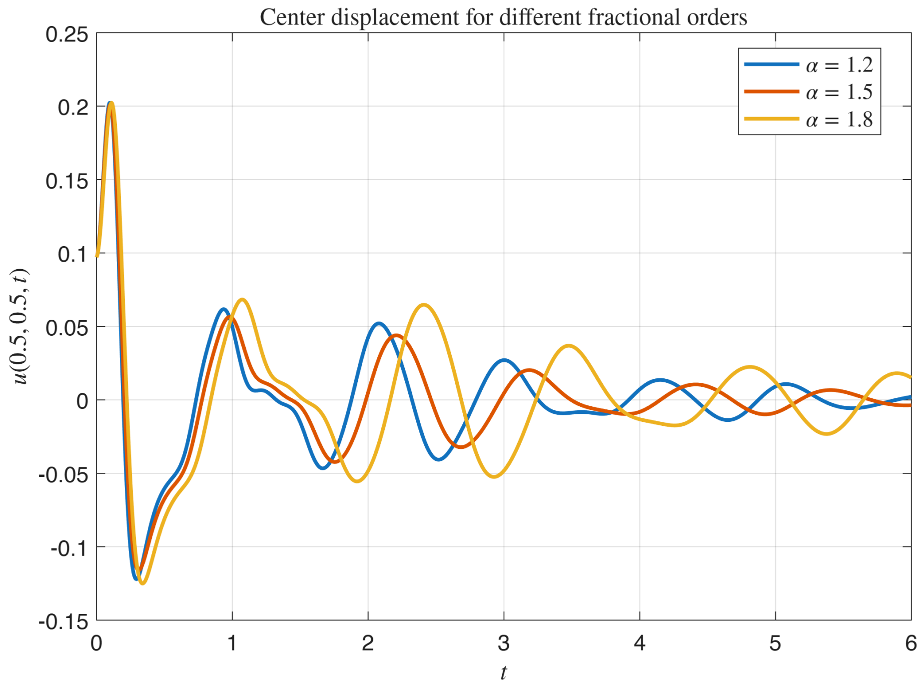

Figure 2. Displacement at the observation point $(0.5, 0.5)$ for different fractional orders in Example 4.

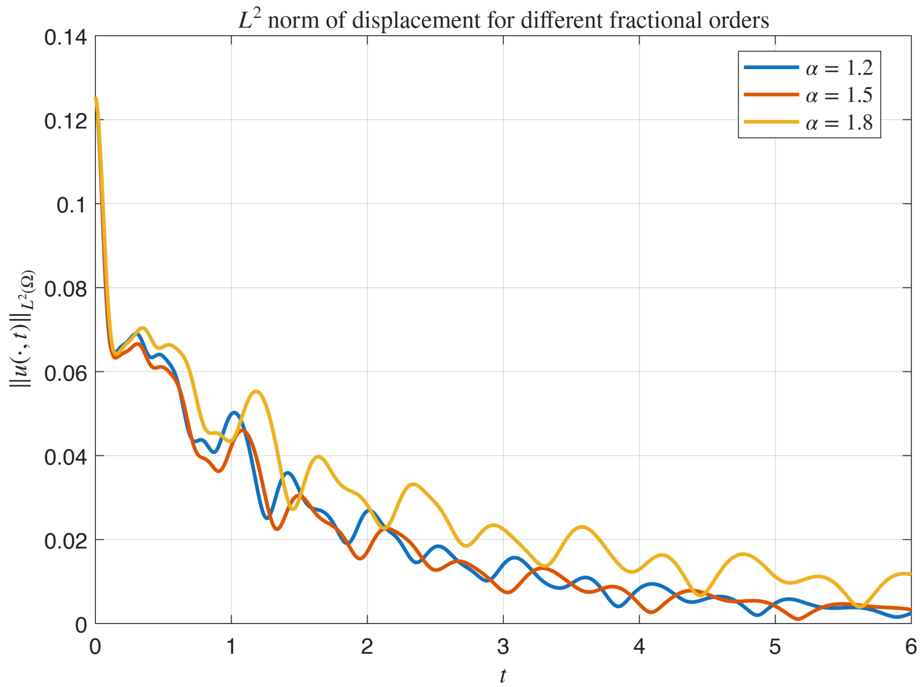

Figure 3. Time evolution of the L^2-norm of the displacement for different fractional orders in Example 4.

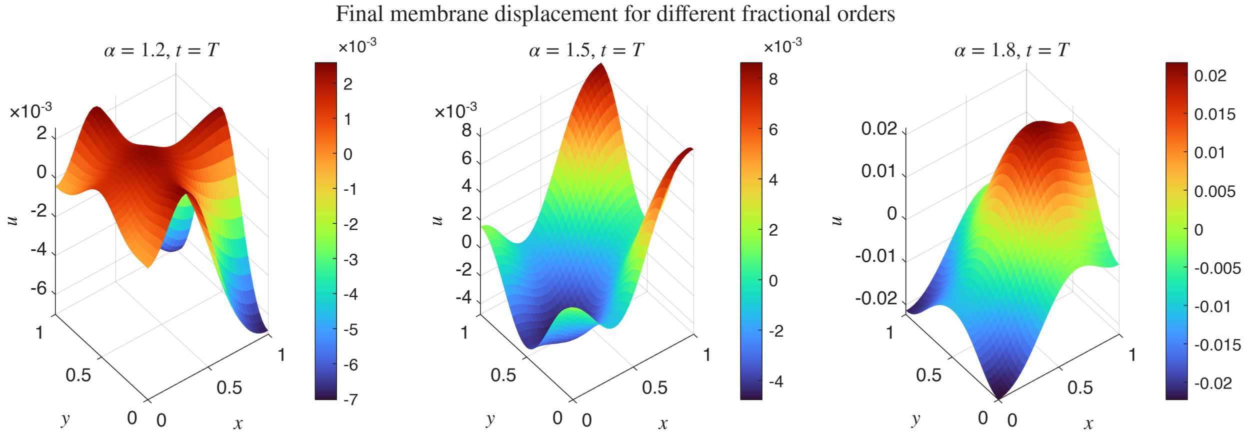

Figure 4. Final-time displacement profiles for different fractional orders in Example 4.

5.5. Example 5: Modal analysis of a fractional viscoelastic membrane

We finally consider the modal response analysis. This example is not a convergence test, but an application-oriented demonstration of how the Caputo acceleration memory term affects different vibration modes.

We solve

$$\partial_t^2 u + k\, {}^C D_{0+}^{\alpha} u - \Delta u = 0 \quad \text{in } \Omega \times (0, T),$$

with

$$\Omega = (0, 1)^2, \qquad T = 10, \qquad k = 0.5,$$

and homogeneous Neumann boundary conditions. The spatial discretization uses continuous piecewise linear finite elements on a uniform triangular mesh.

Let $\mathbf{M}$ and $\mathbf{K}$ be the finite element mass and stiffness matrices. We solve

$$\mathbf{K}\boldsymbol{\phi}_{h,j} = \lambda_{h,j}\mathbf{M}\boldsymbol{\phi}_{h,j}, \qquad \boldsymbol{\phi}_{h,i}^T\mathbf{M}\boldsymbol{\phi}_{h,j} = \delta_{ij}.$$

The first Neumann eigenvalue corresponds to the constant mode and is omitted from the modal plots. Since some eigenvalues on the square have a multiplicity greater than one, Figure 5 displays the selected representative non-constant modes.

Expanding

$$u_h(t) = \sum_j q_j(t)\boldsymbol{\phi}_{h,j},$$

each modal coefficient satisfies

$$q_j''(t) + k\, {}^C D_{0+}^{\alpha} q_j(t) + \lambda_{h,j} q_j(t) = 0.$$

With $z_j = q_j'$ and $\beta = \alpha - 1$, we obtain

$$z_j'(t) + k\, {}^C D_{0+}^{\beta} z_j(t) + \lambda_{h,j} q_j(t) = 0, \qquad q_j'(t) = z_j(t).$$

The same L1 discretization is applied to this scalar modal system.

We select three representative non-constant modes corresponding to low, intermediate, and relatively high spatial frequencies. For each mode, we have

$$q_j(0) = 1, \qquad z_j(0) = 0.$$

The fractional orders $\alpha = 1.2, 1.5, 1.8$ are compared.

Figure 5 shows the selected eigenmodes, while Figure 6 reports the modal amplitudes. The results show that the fractional order changes both the attenuation and phase of modal oscillations. To further illustrate the modal decay, we plot the normalized indicator

$$E_j(t) = \frac{1}{2}\left(|z_j(t)|^2 + \lambda_{h,j}|q_j(t)|^2\right), \qquad \frac{E_j(t)}{E_j(0)}.$$

This quantity is used only as a numerical indicator of the modal amplitude decay, since the true fractional energy includes nonlocal memory contributions. Figure 7 shows that the attenuation depends on both the fractional order and the spatial frequency.

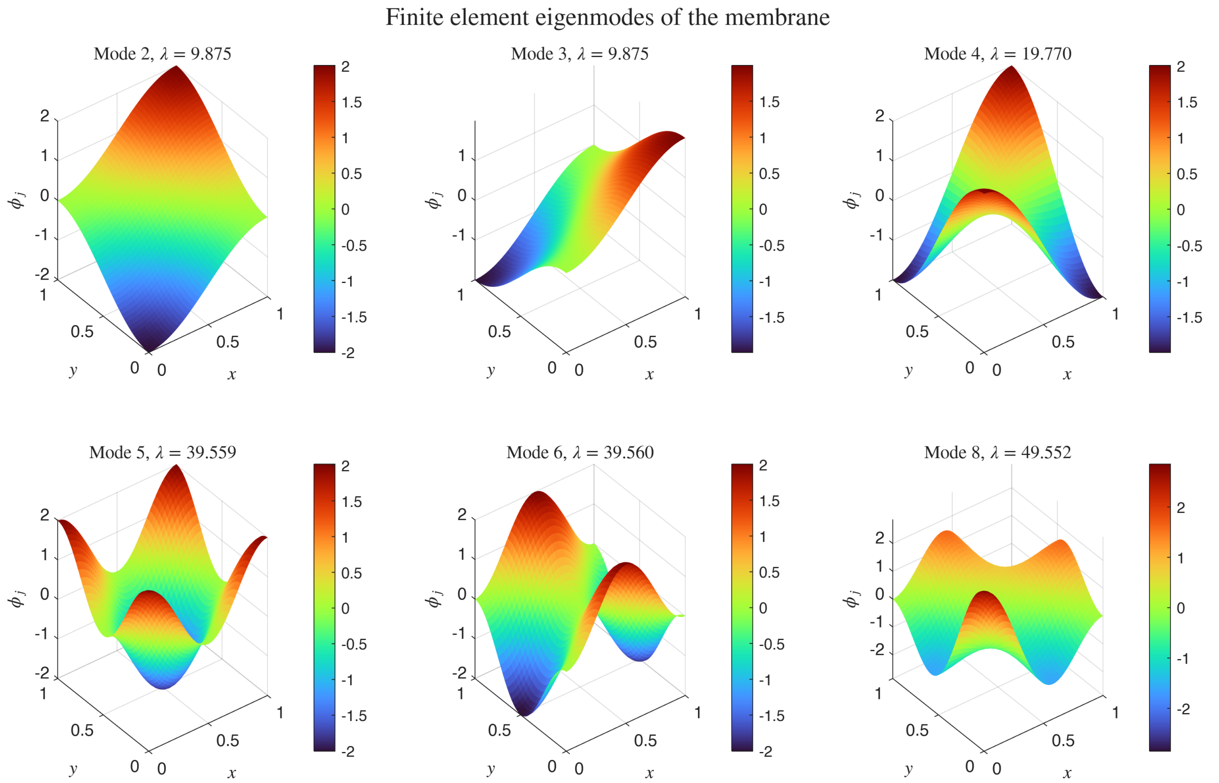

Figure 5. Selected finite element eigenmodes of the membrane in Example 5. The constant Neumann mode is omitted, and representative non-constant modes are displayed.

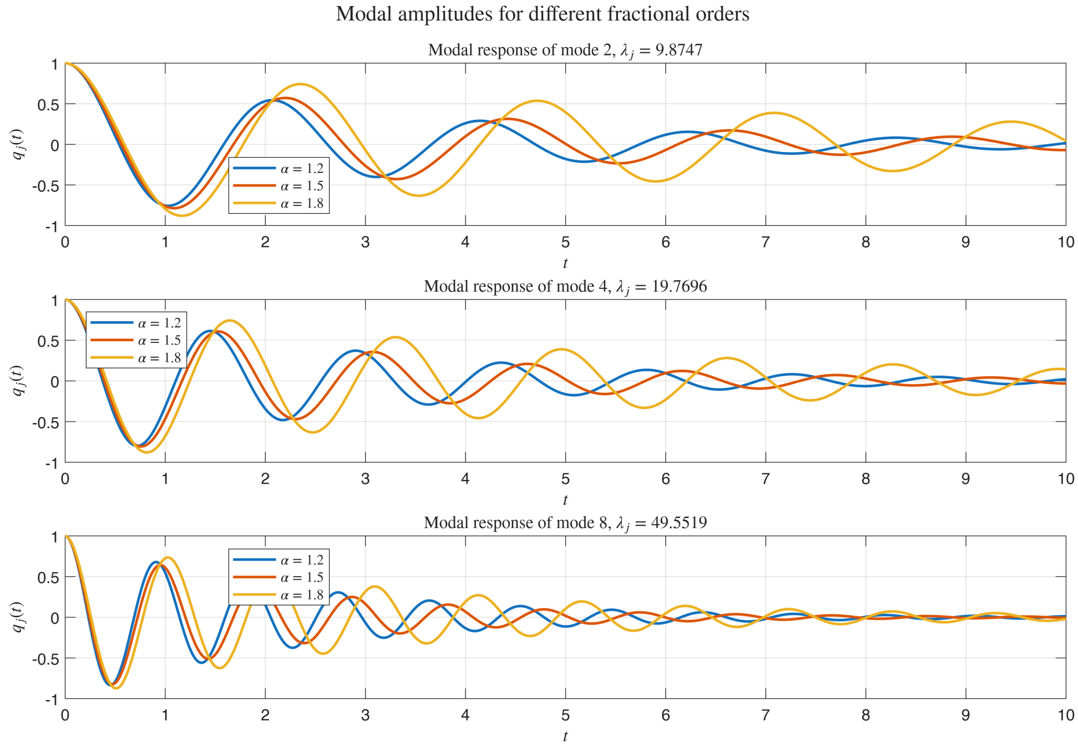

Figure 6. Modal amplitudes for different fractional orders in Example 5.

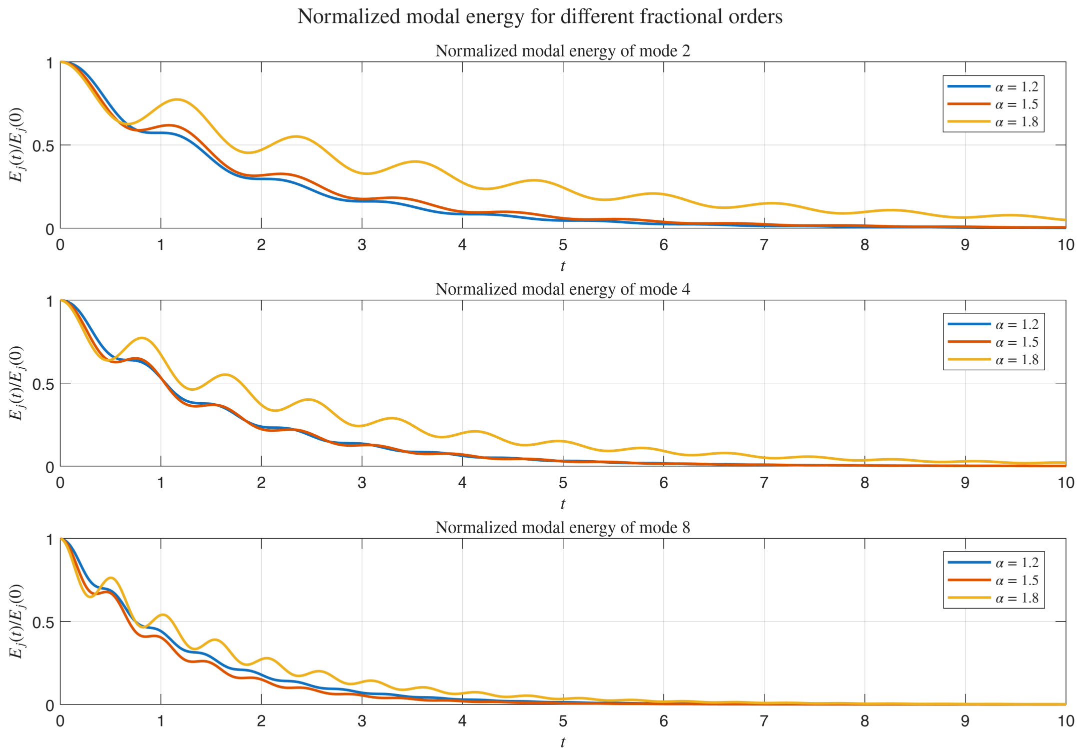

Figure 7. Normalized modal energy-like numerical indicators for different fractional orders in Example 5.

5.6. Discussion

The numerical experiments support the theoretical and practical properties of the proposed order-reduced L1 finite element method. Example 1 confirms the predicted first order temporal and second-order spatial convergence under homogeneous Neumann boundary conditions. Example 2 shows that the same framework also applies to homogeneous Robin boundary conditions. Example 3 verifies stability and accuracy when the initial velocity is nonzero, which is particularly relevant for the acceleration memory model.

Examples 4 and 5 demonstrate the applicability of the method beyond manufactured solutions. The simulations show that the fractional order significantly affects the temporal attenuation, phase evolution, and spatial vibration patterns. The modal experiments further also indicate that the acceleration memory term induces frequency-dependent damping behavior, consistent with viscoelastic memory effects.

Finally, the manufactured source terms in Examples 1–3 are constructed according to the acceleration-memory Caputo model. Treating the fractional term as a velocity memory contribution would lead to different right-hand sides and a different consistency structure, highlighting the importance of the order-reduced formulation used in this work.

6. Concluding remarks

This paper studied a viscoelastic membrane equation with a Caputo fractional derivative of order $\alpha \in (1, 2)$, where the term

$$^{C}D^{\alpha}_{0+}u = J^{2-\alpha}_{0+}\partial_t^2 u$$

models acceleration history memory and differs from conventional velocity memory damping formulations. By introducing $z = \partial_t u$ and $\beta = \alpha - 1$, the problem was reformulated as an order-reduced system with a Caputo derivative of order $\beta \in (0, 1)$ acting on the velocity. This provides a convenient framework for well-posedness analysis, regularity, numerical discretization, and error estimation.

For Neumann boundary conditions, a shifted spectral scale $\rho_j = (1 + \Lambda_j)^{1/2}$ was introduced to incorporate the zero eigenvalue and treat the constant and positive modes uniformly. The formulation also covers homogeneous Robin boundary conditions through the corresponding elliptic bilinear form. A fully discrete finite element method combining the L1 time approximation and continuous piecewise linear finite elements was developed. Under suitable regularity and compatibility assumptions, the method satisfies

$$\|u - U\|_{\widehat{L^\infty}(L^2)} + \|\partial_t u - Z\|_{\widehat{L^\infty}(L^2)} \le C(\tau + h^2).$$

Numerical experiments confirm the predicted first-order convergence in time and second-order convergence in space. The Robin boundary and nonzero initial velocity tests further verify the applicability and stability of the proposed order-reduced framework. Simulations with localized initial perturbations illustrate the effect of the fractional order on membrane vibration, while the modal response experiments show frequency-dependent damping induced by acceleration memory.

Future work may include graded or adaptive temporal meshes for weak initial singularities, higher-order convolution quadrature or Alikhanov-type discretizations with suitable correction strategies, fast convolution algorithms for long-time simulations, and extensions to nonlinear viscoelastic membrane or plate models with fractional acceleration memory effects.

Use of AI tools declaration

The authors declare they have not used artificial intelligence (AI) tools in the creation of this article.

Acknowledgments

This research was partially supported by the National Key R&D Program of China (No. 2024YFF0507903), the National Natural Science Foundation of China (Nos. 12401555, and 52509151), the China Postdoctoral Science Foundation (No. 2025M783290), the Shandong Provincial Natural Science Foundation (Nos. ZR2025LZN010, ZR2025QC1111, and ZR2025MS743), the Taishan Scholars Program of Shandong Province (Nos. tsqn202507039, tsqn202408001, and tsqn202312053), and the Shandong University Undergraduate Education Reform Project (Grant No. 2025Z31).

Conflict of interest

The authors declare there are no conflicts of interest.

References

1. M. Ansari, E. Esmailzadeh, D. Younesian, Internal-external resonance of beams on non-linear viscoelastic foundation traversed by moving load, *Nonlinear Dyn.*, **61** (2010), 163–182. https://doi.org/10.1007/s11071-009-9639-0
2. D. J. Inman, R. C. Singh, *Engineering Vibration*, Prentice Hall, Englewood Cliffs, NJ, 1994.
3. L. Meirovitch, *Fundamentals of Vibrations*, Waveland Press, Long Grove, IL, 2010.
4. S. Timoshenko, D. H. Young, W. Weaver, *Vibration Problems in Engineering*, John Wiley & Sons, New York, 1974.
5. R. M. Christensen, *Theory of Viscoelasticity: An Introduction*, Academic Press, New York, 1982.
6. M. Fabrizio, B. Lazzari, On the existence and the asymptotic stability of solutions for linearly viscoelastic solids, *Arch. Ration. Mech. Anal.*, **116** (1991), 139–152. https://doi.org/10.1007/BF00375589
7. M. Fabrizio, A. Morro, *Mathematical Problems in Linear Viscoelasticity*, SIAM, Philadelphia, 1992. https://doi.org/10.1137/1.9781611970807
8. R. L. Bagley, Power law and fractional calculus model of viscoelasticity, *AIAA J.*, **27** (1989), 1412–1417. https://doi.org/10.2514/3.10279
9. R. L. Bagley, P. J. Torvik, A theoretical basis for the application of fractional calculus to viscoelasticity, *J. Rheol.*, **27** (1983), 201–210. https://doi.org/10.1122/1.549724
10. A. Bonfanti, J. L. Kaplan, G. Charras, A. Kabla, Fractional viscoelastic models for power-law materials, *Soft Matter*, **16** (2020), 6002–6020. https://doi.org/10.1039/D0SM00354A
11. C. Li, F. Zeng, *Numerical Methods for Fractional Calculus*, Chapman and Hall/CRC, Boca Raton, 2015. https://doi.org/10.1201/b18503

12. F. Mainardi, *Fractional Calculus and Waves in Linear Viscoelasticity: An Introduction to Mathematical Models*, World Scientific, Singapore, 2010. https://doi.org/10.1142/p614

13. F. Mainardi, G. Spada, Creep, relaxation and viscosity properties for basic fractional models in rheology, *Eur. Phys. J. Spec. Top.*, **193** (2011), 133–160. https://doi.org/10.1140/epjst/e2011-01387-1

14. Y. A. Rossikhin, M. V. Shitikova, Application of fractional calculus for dynamic problems of solid mechanics: novel trends and recent results, *Appl. Mech. Rev.*, **63** (2010), 010801. https://doi.org/10.1115/1.4000563

15. K. Diethelm, *The Analysis of Fractional Differential Equations*, Springer, Berlin, 2010. https://doi.org/10.1007/978-3-642-14574-2

16. R. Gorenflo, F. Mainardi, Fractional calculus: integral and differential equations of fractional order, in *Fractals and Fractional Calculus in Continuum Mechanics*, Springer, Vienna, (1997), 223–276. https://doi.org/10.1007/978-3-7091-2664-6_5

17. A. A. Kilbas, H. M. Srivastava, J. J. Trujillo, *Theory and Applications of Fractional Differential Equations*, Elsevier, Amsterdam, 2006.

18. I. Podlubny, *Fractional Differential Equations*, Academic Press, San Diego, 1999.

19. S. G. Samko, A. A. Kilbas, O. I. Marichev, *Fractional Integrals and Derivatives: Theory and Applications*, Gordon and Breach, London, 1993.

20. B. Jin, R. Lazarov, Z. Zhou, An analysis of the L1 scheme for the subdiffusion equation with nonsmooth data, *IMA J. Numer. Anal.*, **36** (2016), 197–221. https://doi.org/10.1093/imanum/dru063

21. B. Jin, B. Li, Z. Zhou, Correction of high-order BDF convolution quadrature for fractional evolution equations, *SIAM J. Sci. Comput.*, **39** (2017), A3129–A3152. https://doi.org/10.1137/17M1118816

22. H. L. Liao, D. Li, J. Zhang, Sharp error estimate of the nonuniform L1 formula for linear reaction-subdiffusion equations, *SIAM J. Numer. Anal.*, **56** (2018), 1112–1133. https://doi.org/10.1137/17M1131829

23. H. L. Liao, W. McLean, J. Zhang, A discrete Gronwall inequality with applications to numerical schemes for subdiffusion problems, *SIAM J. Numer. Anal.*, **57** (2019), 218–237. https://doi.org/10.1137/16M1175742

24. Y. Lin, C. Xu, Finite difference/spectral approximations for the time-fractional diffusion equation, *J. Comput. Phys.*, **225** (2007), 1533–1552. https://doi.org/10.1016/j.jcp.2007.02.001

25. C. Lubich, Discretized fractional calculus, *SIAM J. Math. Anal.*, **17** (1986), 704–719. https://doi.org/10.1137/0517050

26. C. Lubich, Convolution quadrature and discretized operational calculus. I, *Numer. Math.*, **52** (1988), 129–145. https://doi.org/10.1007/BF01398686

27. M. Stynes, E. O'Riordan, J. L. Gracia, Error analysis of a finite difference method on graded meshes for a time-fractional diffusion equation, *SIAM J. Numer. Anal.*, **55** (2017), 1057–1079. https://doi.org/10.1137/16M1082329

28. Y. Feng, L. Li, J. G. Liu, T. Tang, Some Gronwall inequalities for a class of discretizations of time fractional equations on nonuniform meshes, *SIAM J. Numer. Anal.*, **62** (2024). https://doi.org/10.1137/24M1631614

29. C. Quan, X. Wu, L^2-norm stability and convergence of an L2-type method on nonuniform meshes for subdiffusion equation, *SIAM J. Numer. Anal.*, **61** (2023), 2586–2611. https://doi.org/10.1137/22M1506468

30. B. Jin, Q. Quan, B. Wohlmuth, Z. Zhou, Regularity analysis and high-order time stepping scheme for quasilinear subdiffusion, *SIAM J. Numer. Anal.*, **63** (2025). https://doi.org/10.1137/23M159531X

31. M. López-Fernández, L. Płociniczak, Convolution quadrature for the quasilinear subdiffusion equation, *SIAM J. Numer. Anal.*, **63** (2025). https://doi.org/10.1137/23M161450X

32. X. J. Li, C. J. Xu, A space-time spectral method for the time fractional diffusion equation, *SIAM J. Numer. Anal.*, **47** (2009), 2108–2131. https://doi.org/10.1137/080718942

33. K. Mustapha, Time-stepping discontinuous Galerkin methods for fractional diffusion problems, *Numer. Math.*, **130** (2015), 497–516. https://doi.org/10.1007/s00211-014-0669-2

34. Z. Z. Sun, X. Wu, A fully discrete difference scheme for a diffusion-wave system, *Appl. Numer. Math.*, **56** (2006), 193–209. https://doi.org/10.1016/j.apnum.2005.03.003

35. H. Yuan, X. Xie, A fast fully discrete mixed finite element scheme for fractional viscoelastic models of wave propagation, *Numer. Math. Theory Methods Appl.*, **19** (2026), 129–154. https://doi.org/10.4208/nmtma.OA-2025-0030

36. X. Zheng, H. Wang, Analysis and discretization of a variable-order fractional wave equation, *Commun. Nonlinear Sci. Numer. Simul.*, **104** (2022), 106047. https://doi.org/10.1016/j.cnsns.2021.106047

37. X. Zheng, H. Wang, A hidden-memory variable-order fractional optimal control model: analysis and approximation, *SIAM J. Control Optim.*, **59** (2021), 1851–1880. https://doi.org/10.1137/20M1344962

38. X. Zheng, H. Wang, An error estimate of a numerical approximation to a hidden-memory variable-order space-time fractional diffusion equation, *SIAM J. Numer. Anal.*, **58** (2020), 2492–2514. https://doi.org/10.1137/20M132420X

39. X. Zheng, H. Wang, Optimal-order error estimates of finite element approximations to variable-order time-fractional diffusion equations without regularity assumptions of the true solutions, *IMA J. Numer. Anal.*, **41** (2021), 1522–1545. https://doi.org/10.1093/imanum/draa013

40. X. Zheng, H. Wang, An optimal-order numerical approximation to variable-order space-fractional diffusion equations on uniform or graded meshes, *SIAM J. Numer. Anal.*, **58** (2020), 330–352. https://doi.org/10.1137/19M1245621

41. X. Zheng, Two methods addressing variable-exponent fractional initial and boundary value problems and Abel integral equation, *CSIAM Trans. Appl. Math.*, **6** (2025), 666–710. https://doi.org/10.4208/csiam-am.SO-2024-0052

42. X. Zheng, Z. Yang, W. Li, H. Wang, A time-fractional mean field control modeling subdiffusive advective transport, *SIAM J. Sci. Comput.*, **45** (2023), B884–B905. https://doi.org/10.1137/22M1527726

43. W. McLean, *Strongly Elliptic Systems and Boundary Integral Equations*, Cambridge University Press, Cambridge, 2000.